Modeling The States of Liquid Phase Change Pouch Actuators by Reservoir Computing

Cedric Caremel[1,†], Khang Nguyen[2,†], Anh Nguyen[3], Manfred Huber[2], Yoshihiro Kawahara[1], and Tung D. Ta[4]

***Abstract*— Liquid phase change pouch actuators (liquid pouch motors) hold great promise for a wide range of robotic applications, from artificial organs to pneumatic manipulators for dexterous manipulation. However, the usability of liquid pouch motors remains challenging due to the nonlinear intrinsic properties of liquids and their highly dynamic implications for liquid-gas phase changes, which complicate state modeling and estimation. To address these issues, we propose a reservoir computing-based method for modeling the inflation states of a customized liquid pouch motor, which serves as an actuator, featuring four Peltier heating junctions. We use a motion capture system to track the landmark movements on the pouch as a proxy for its volumetric profile. These movements represent the internal liquid-gas phase changes of the pouch at stable room temperature, atmospheric pressure, and in the presence of electrical noise. The motion coordinates are thus learned by our reservoir computing framework, *PhysRes*, to model the states based on prior observations. Through training, our model achieves excellent results on the test set, with a normalized root mean squared error of 0.0041 in estimating the states and a corresponding volumetric error of 0.0160%. To further demonstrate how such actuators could be implemented in the future, we also design a dual-pouch actuator-based robotic gripper to control the grasping of soft objects. Our design and source code are available at: https://github.com/tatung/liquidpouch_reservoir.**

I. INTRODUCTION

Liquid phase change pouch actuators are utilized in various applications, including soft robotics, tangible interfaces, and haptics, due to their advantages in compact size, high force output, and ease of fabrication. However, due to the nonlinearity in both liquid-gas phase transitions and deformable structures, it remains challenging to model and control the behavior of these actuators. In most applications, the control of these actuators is open-loop and heavily relies on empirical, heuristic trial-and-error. The difficulties in modeling and controlling soft actuators make it challenging to design robust and reliable soft robotic systems with greater granularity in the motion of liquid phase change pouch actuators. In this paper, the "deformation" of the liquid pouch governs the highly nonlinear behavior of the inflation of a liquid-based, phase-change, actuator. The observed nonlinearities exhibit hysteresis-like behavior (characterized by time dependency), making it difficult to capture them with traditional analytical models. To address this challenge, we adopt a data-driven approach following the principles of a physical reservoir computing (PRC), *PhysRes* [1], where the complex dynamics of a physical system (here, our actuated pouch) is used for computation. Importantly, in this work, we primarily focus on modeling the nonlinear phase changes in a latent space or "states". In return, this state space is what allows us to model the essential underlying physical configuration and dynamics of the future system state. Since the reservoir's internal state space is used to learn a latent representation of the actuator's underlying physical configuration from sensor data, we can effectively model the system's complex memory effects without an explicit first-principles physical model.

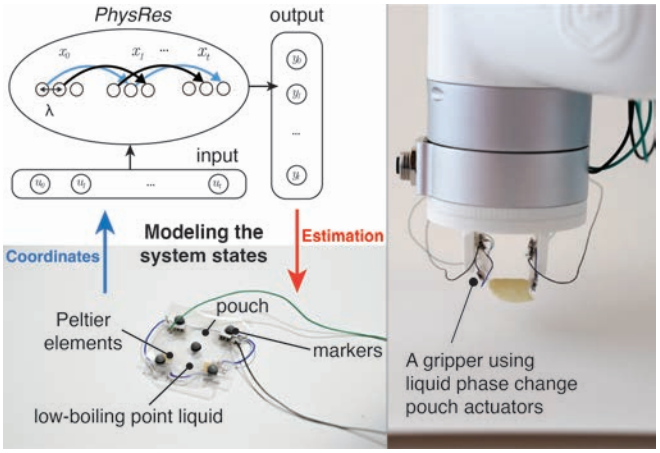

Fig. 1: Left: The overall pipeline includes collecting, estimating, and modeling the states of a liquid phase change actuator using a reservoir computing model. **Right**: The liquid phase change pouch actuators are applied to make a soft robotic gripper that can delicately grasp a fragile object.

Soft Pneumatic Actuator: Soft pneumatic actuators have been widely explored. This line of work is primarily based on the volumetric state changes of a deformable bag caused by changing the pressure inside and outside the chamber [2],

*This work was supported by JSPS Grant-in-Aid for Scientific Research (B) Grant Number 23H01376, Japan, the Royal Society ISPF International Collaboration Awards 2023 (Japan) ICA\R1\231067, and Hirose Foundation Research Grant.

† Authors have equal contributions.

[1]Graduate School of Engineering, The University of Tokyo, 7-3-1 Hongo, Bunkyo-ku, Tokyo, Japan {cedric, kawahara}@akg.t.u-tokyo.ac.jp

[2]Department of Computer Science and Engineering, University of Texas at Arlington, USA khang.nguyen8@mavs.uta.edu, huber@cse.uta.edu

[3]Department of Computer Science, University of Liverpool, UK anh.nguyen@liverpool.ac.uk

[4]Graduate School of Information Science and Technology, The University of Tokyo, 7-3-1 Hongo, Bunkyo-ku, Tokyo, Japan tung@csg.ci.i.u-tokyo.ac.jp

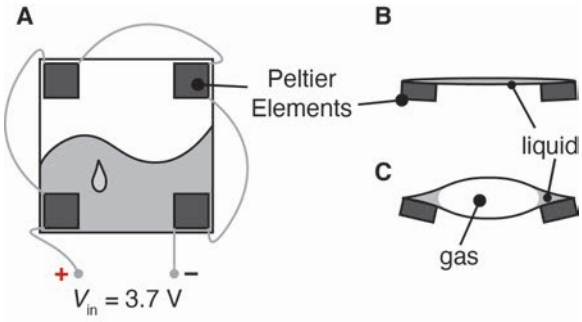

Fig. 2: The design of a square liquid pouch motor. **(A)** The liquid pouch motor is a square pouch filled with a low-boiling point liquid. Four Peltier elements are attached to four corners of the square pouch. **(B)** Side-view of a deflated liquid phase change pouch actuator. **(C)** The inflating liquid pouch during the liquid-gas phase transition where part of the liquid gathers at the pouch edges.

[3], [4]. An external compressor pump typically controls the pressure inside the chamber through a medium, such as gas or liquid. The chamber's shape is varied, such as bellow shapes [5], digitated shapes [6], and long tubes [7]. The early work of Pouch Motor [8] introduced a computational approach to designing the shape of the pneumatic actuator. Therefore, this research enabled the development of various rapid-prototyping soft pneumatic actuators based on the inflation and deflation of a nylon pouch.

Liquid Phase Change Pouch Actuators: The liquid phase change pouch actuators work based on the volumetric change due to the liquid-gas phase change of the liquid inside the actuator [9]. A typical method for triggering this phase change is through thermal cycling. The work in [10] combined the pneumatic pouch motor design in [8] with a low-boiling-point liquid to enable rapid prototyping of a liquid phase change pouch actuator. Meanwhile, other researchers extend the concept of the liquid phase change pouch motor to different types of materials to make the chamber [11] and various ways of thermally triggering the phase change [12], [13]. Because of their compact size and strong exerted force, liquid pouch actuators are used in applications such as a soft haptic display [14] and an origami jumper [15]. However, due to the nonlinearity of the thermal cycling process and the deformability of the pouch, it remains a challenge to model and control liquid-phase-change pouch actuators.

Reservoir Computing (RC) for Soft-Bodied Robots: Reservoir computing has been widely adopted in the soft robotics community in recent years thanks to its ability to handle complex, nonlinear dynamics efficiently with minimal computational overhead via echo state networks (ESNs) [16], [17], [18], [19] and liquid state machines (LSMs) [20], [21]. Flexible material-based robots first utilized ESNs for controlling the seminal octopus arm [22], [23], [24]. Taking a step forward, ESNs are further employed on pneumatic artificial muscle [25], [26] and SMA-based bending robots for sensorimotor learning [16]. However, the large-scale development of soft robotics is not only focused on flexible, deformable, and rigid materials, but also on non-rigid bodies, which are not yet well-explored, specifically for liquid-based actuators. These robots make control uncertainty and state estimation more challenging because of the unpredictable phase changes in the underlying liquid materials.

Our contributions are layered as follows:

- *Design*: We design a liquid phase change pouch actuator driven by Peltier elements that is proven to work under electrical current.
- *Pipeline*: We develop a pipeline for collecting positional and volumetric data for estimating liquid phase change pouch actuators.
- *State Modeling and Estimation*: We theoretically and empirically model and estimate the state of the liquid phase change pouch actuators using a reservoir computing-based approach.
- *Application*: We apply our design and the proposed framework together to build a soft robotic gripper based on liquid phase change actuation with the capability to grab and pick up fragile objects.

II. DESIGN OF A LIQUID POUCH ACTUATOR

As mentioned earlier, the liquid pouch actuator operates based on the liquid-gas phase transition of the liquid inside the plastic pouch. In this work, we design a square pouch with a size of $20\,\mathrm{mm} \times 20\,\mathrm{mm}$. The pouch is fabricated by sealing two nylon sheets using a heat sealer. We then fill the pouch with $V_0 = 0.02\,\mathrm{mL}$ of low-boiling point ($61\,^\circ\mathrm{C}$) liquid Noah 7100 [27] as illustrated in Fig. 1. Table I shows the values of the liquid pouch actuator's morphology parameters, including the parametric parameters used for fabrication.

TABLE I: Our parametric design of the liquid pouch actuator with pouch size in millimeters (mm), liquid volume in milliliters (mL), pouch material, and low-boiling-point liquid.

Parameter	Value
Pouch Size (L)	$20\,\mathrm{mm}$
Liquid Volume (V_0)	$0.02\,\mathrm{mL}$
Pouch Material	ONy15/L-LDPE[1]
Low-boiling Point Liquid	Noah 7100 [27]

To actuate the liquid pouch actuator, we heat the liquid inside the pouch to its boiling point ($61\,^\circ\mathrm{C}$ for Noah 7100). The input signal corresponds to the heating power applied to the pouch via four Peltier elements with [28] size of $3.96\,\mathrm{mm} \times 3.96\,\mathrm{mm} \times 2.40\,\mathrm{mm}$ attached to one side at the four corners of the liquid pouch actuators (as shown in Fig. 2). In our modeling framework, the input signal to the reservoir computing model is derived from displacement readings captured via the OptiTrack motion tracking system, rather than from electrical signals or sensor measurements internal to the actuator. These displacement inputs reflect the externally observable volumetric deformation of the pouch over time, enabling the reservoir to infer latent dynamic states and predict future behavior. Empirically, we observe that during the inflation process, due to surface tension, the liquid inside the pouch that has not yet vaporized accumulates at the edges and corners of the pouch. We therefore attach the four Peltier elements to the pouch's

four corners, ensuring that the liquid is vaporized during the heating-up phase. Peltier elements are adhered to the pouch using a thin double-sided tape to fix the Peltier elements while maintaining thermal conductivity. Note that four Peltier elements are put in series and connected to a stable 3.7 V DC power source through a MOSFET-based switch.

III. VOLUMETRIC POUCH STATE MODELING & ESTIMATION

A. Estimating Liquid Phase Changes

An ESN can be formally defined as a reservoir of N neurons whose state evolves according to:

$$\mathbf{x}(t) = \sigma(\mathbf{W}_{\text{in}}\mathbf{u}(t) + \mathbf{W}_{\text{res}}\mathbf{x}(t-1)), \tag{1}$$

where $\mathbf{u}(t) \in \mathbb{R}^D$ is the input signal vector, $\mathbf{x}(t) \in \mathbb{R}^N$ is the recurrent layer, $\mathbf{W}_{\text{in}} \in \mathbb{R}^{N\times D}$ is the connection weights from the input layer to the reservoir, $\mathbf{W}_{\text{res}} \in \mathbb{R}^{N\times N}$ is the connecting weights within the reservoir, and $\sigma(\cdot)$ represents nonlinear activation function.

In this work, the relation among the pouch's volumetric states, the input signal, and liquid phase changes is highly nonlinear and time-dependent, which is difficult to approximate. We employed the hysteretic encoding function $\sigma(\cdot)$, which ideally represents these dynamics, together with *PhysRes* [1], a robust approach based on the physical RC for controlling soft actuators (*e.g.*, McKibben pneumatic artificial muscles or PAMs). Specifically, *PhysRes* is superior to ESN by leveraging the nonlinear properties of a hysteretic encoding to estimate future states based on past observations. Hysteretic behavior, denoted by a latency, λ, governs the interaction between system input and output as:

$$\sigma(\zeta_k) = \begin{cases} 0, & \text{if } k < \lambda \\ 1/\left[1 + e^{-\alpha(\zeta_k - \lambda)}\right], & \text{otherwise} \end{cases} \tag{2}$$

Eq. 2 outputs zero, representing the lag when the input vector index k is less than λ; otherwise, it applies its nonlinear activation function, modulated by the scaling parameter α. Here, the system input is interpreted as past observations of the pouch's physical changes, and the system output is used to model the pouch's states. From this, the hysteretic reservoir's state updated at time t is determined by the hysteretic encoding's output, relying on the previous state with a fixed delay τ:

$$\mathbf{x}(t) \coloneqq \sigma(\zeta_k) = \sigma(\mathbf{W}_{\text{in}}\mathbf{u}(t) + \mathbf{x}(t-\tau)) \tag{3}$$

Therefore, Eq. 3 better handles nonlinearity via the hysteretic encoding itself. In addition, the predictive state update only depends on the past state $\mathbf{x}(t-\tau)$ rather than a weighted sum of past activations like in ESN, via getting rid of random internal connectivities $\mathbf{W}_{\text{in}}$ as in Eq. 1. Specifically, the encoding function $\sigma(\cdot)$ captures nonlinear dynamics by transforming input and past states into a high-dimensional, nonlinear representation. In our hysteretic formulation (Eq. 3), the encoder $\sigma(\cdot)$ further embeds memory effects and delayed responses, enabling accurate modeling of time-dependent physical transitions. Thus, the trainable readout weight matrix, W_{out}, is conducted through linear regression with the target $\mathbf{y}$ with the trained weights $\mathbf{W}_{\text{out}}^{+}$:

$$\mathbf{W}_{\text{out}} = \mathbf{W}_{\text{out}}^{+} \cdot \mathbf{y} \tag{4}$$

Subsequent predictions $\hat{\mathbf{y}}$ are derived from the trained state matrix $\mathbf{x}(t)$:

$$\hat{\mathbf{y}} = \mathbf{x}(t) \cdot \mathbf{W}_{\text{out}} \tag{5}$$

The predictions $\hat{\mathbf{y}}$ output by *PhysRes* in Eq. 5 correspond to our aim to estimate the pouch's state.

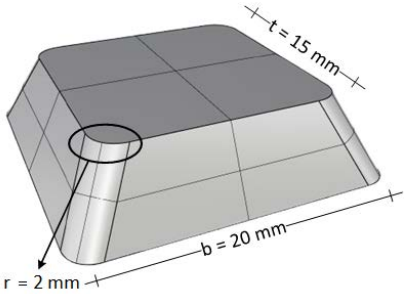

Fig. 3: The pouch inflation is symmetric through the mid-plane, so we only need to estimate the volume of the upper part of the pouch, which is approximated as a round square frustum. In Eq. 7, the integral stacks are the areas of the rounded-corner square from the base to the top of the shape, resulting in the cap's volume.

B. Modeling Inflated Volumetric States with Observations

According to our design specification, the liquid pouch is primarily inflated at the rounded-corner, square-sized regions at both ends, as depicted in Fig. 3. We establish connections between the positional states and the volumetric states of the pouch for further investigation. Note that while modeling the states of our customized liquid pouch, we implicitly assume that the four corners of the pouch are well-positioned on the same plane and unaffected by the pouch's growth. The main interesting point in the pouch is the growing height, which is a good proxy for observing its volumetric change. Although the pouch buckles when the pressure inside exceeds a specific threshold, for the simplicity of the volumetric estimation calculation, we maintain the pressure below the threshold, thereby preventing buckling. We also assume that the inflation of the pouch is symmetric through the mid-plane.

The volume of the inflated pouch can be estimated as twice the volume of the frustum, also known as the pouch cap, as shown in Fig. 3. Presumably, the pouch is defined to be at a rest state when the cap height is zero and to be inflated when the cap height is larger. The dimension of the caps, when being inflated, is considered as a rounded-corner square base, which can be characterized in terms of s as a square dimension and r as the rounded corner radius:

$$A = s^2 + 4rs + \pi r^2 \tag{6}$$

Eq. 6 portrays the cross-sectional area of the pouch's cap only. As the pouch gets inflated, the base dimension is called b, and the top dimension is called t, making the pouch cap's

[1] https://www.kintora.co.jp/html/index.php/rami/

shape a square-round frustum. During the design process of the liquid pouch, the formation of a rounded square geometry (denoted as r in our volumetric calculation) was consistently observed and quantified throughout the inflation phase. This empirical observation remained reproducible across multiple experimental trials and formed our geometric approximation.

By stacking the rounded-squared squares, its inflated volume, ΔV_+, is calculated via the integration along the growing height h with the sliced area functions $A(z)$:

$$\begin{aligned}\Delta V_+ &= 2\int_0^h A(z)\ dz = 2\int_0^h s(z)^2 + 4rs(z) + \pi r^2 \\ &= 2\int_0^h \left[(b + \frac{z(t-b)}{h}\right]^2 + 4r\left[b + \frac{z(t-b)}{h}\right] + \pi r^2 \\ &= \frac{2h}{3}(b^2 + bt + t^2 + 6rb + 6rt + 3\pi r^2)\end{aligned} \tag{7}$$

Given the dimension of $b = 20\,\text{mm}$, $t = 15\,\text{mm}$, and $r = 2\,\text{mm}$ as shown in Fig. 3, Eq. 7 is simplified to:

$$\Delta V_+ = \frac{(2690 + 24\pi)}{3} h\ (\text{mm}^3) \tag{8}$$

With continuous height measurements, we estimate the liquid pouch's inflated volume profile instantaneously. Within the scope of this work, we consider pouch states with a continuous spectrum of the inflated volume. The maximal inflated volume of the pouch is depicted as the growing height reaches its maximum value. Coupling the predictive outcomes of Eq. 5 and the computed volume in Eq. 8, we map the coordinate states back into volumetric states of the robot pouch.

IV. EXPERIMENTS & EVALUATIONS

In this section, we evaluate the performance of the liquid pouch actuator inflation, given an initial set of coordinates with our *PhysRes* framework. We conduct offline training and testing experiments and deploy the liquid pouch actuator in real-world experiments.

A. Experiment Set-up

1) Hardware Set-up: The motion capture system OptiTrack [2] is deployed to track the embedded reflective markers on the pouch actuator with micrometer precision. This system provides a labeled state representation for controlling the liquid pouch *during offline experiments* and serves as visual feedback *during online experiments*. In specific, we utilize an OptiTrack setup consisting of three cameras to track the inflation and deflation behavior of a liquid pouch actuator in a controlled cubic workspace of $0.6\,\text{m} \times 0.6\,\text{m} \times 0.6\,\text{m}$. The liquid pouch actuator has a dimension of $20\,\text{mm} \times 20\,\text{mm}$ and is equipped with five $3\,\text{mm}$-semisphere reflective markers: four markers at the corners and one at the center of the pouch, which are used to approximate the skeleton of the actuator as it undergoes cyclic volume inflation and deflation.

[2] https://www.optitrack.com/cameras/

TABLE II: Training hyperparameters for our *PhysRes* model, including reservoir size in number of neurons N, scale α, latency λ, state delay τ, and initial condition x_0.

Hyperparameters	Value
Reservoir Size (N)	1000
Scale (α)	1
Latency (λ)	1
State Delay (τ)	1
Initial Condition (x_0)	0

2) Data Collection: We first collect our dataset on different liquid pouches of the same size to avoid internal design bias, such as geometric patterns, marker locations, and the intrinsic physical property of liquid-gas phase change. These properties are sensitive and can vary among pouches due to design imperfections. In each data collection phase, the positions of the markers are precisely recorded at $120\,\text{Hz}$ with OptiTrack reported accuracy of $0.2\,\text{mm}$.

3) Implementation Details: We also outline the hyperparameter configuration in Table II, detailing the default values we used for reservoir size, scaling factor, latency, state delay, and initial conditions that shape our model operational dynamics, resulting in rapid offline training procedure (in mere seconds on an Apple MacBook Pro M3). In Section III, the input signal $u(t) \in \mathbb{R}^D$ encodes both control commands and environmental conditions, while the state vector $x(t) \in \mathbb{R}^N$ represents the latent volumetric configuration of the pouch. The hysteretic encoding function $\sigma(\cdot)$ maps input-driven variations and delayed physical responses into nonlinear internal states, thereby enabling the model to capture phase transitions and memory-dependent dynamics.

B. Evaluation Metrics

1) Markers Displacement Error: The network can be easily optimized to learn the task as only two primary hyperparameters (λ, α) are used. Therefore, the network's estimation of the states is determined by Normalized Root Mean Square Error (NRMSE):

$$\texttt{NRMSE}(\mathbf{y}, \hat{\mathbf{y}}) = \sqrt{\frac{\sum_k (\mathbf{y}_k - \hat{\mathbf{y}}_k)^2}{\texttt{Var}(\mathbf{y})}} \tag{9}$$

In Eq. 9, $\mathbf{y}$ and $\hat{\mathbf{y}}$ are, therefore, interpreted as the actual and estimated states, respectively.

2) Volumetric Error: Thus, by using Eq. 8, we determine the volume for both the target and the estimated states. To verify the estimated volumetric estimation, we compute the absolute percentage of the volumetric error, $\mathbb{E}$, between the expected volume, $\hat{V}$, and the target volume, V, as follows:

$$\mathbb{E}\left[V, \hat{V}\right] = 100\left|\frac{\hat{V} - V}{V}\right| \tag{10}$$

For the experiments, we use the median to provide a more robust estimation of the typical estimations of markers displacement (Eq. 9) and volumetric errors (Eq.10).

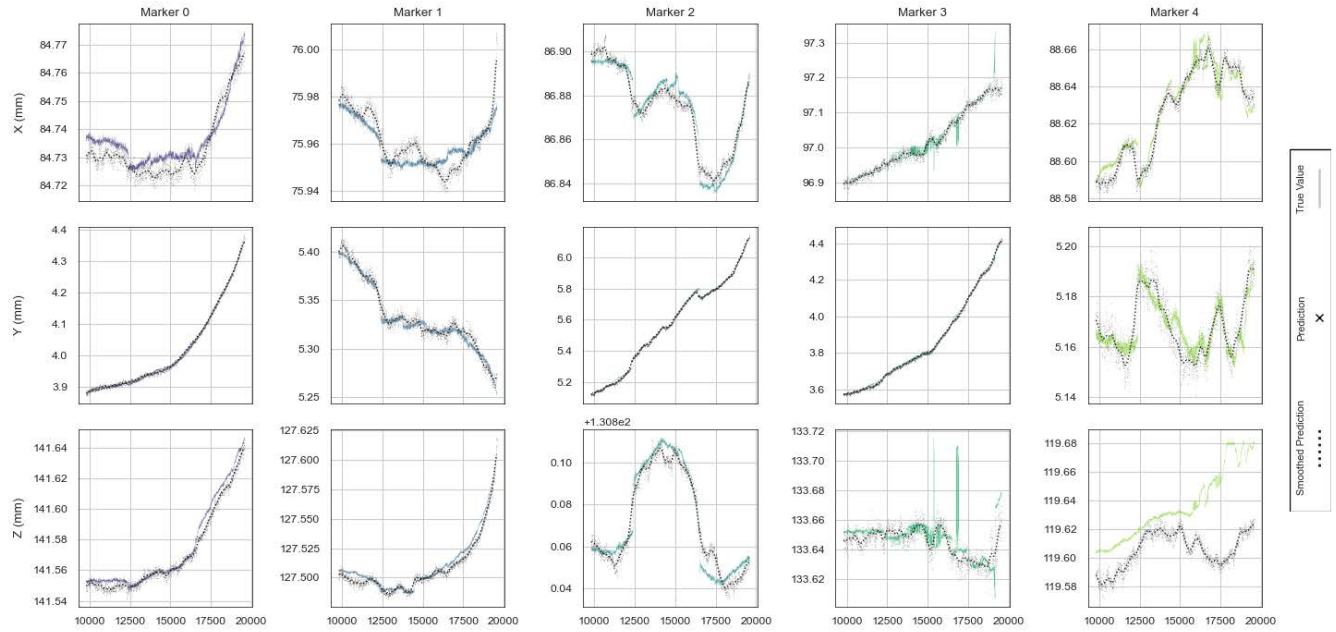

Fig. 4: *PhysRes*'s estimation on a segment in our collected test dataset for offline experiments: past positional observations of five markers are recorded, and our reservoir model makes state estimations, which we smooth out with Gaussian kernel (dashed lines in black), closely matching the ground truth for each marker (each represented by a different colored line). The estimations are made along time steps ranging from 0 to 19587 along the horizontal axis, with each displacement calculated in mm along the vertical axis. Our trained *PhysRes* generates good state estimations in terms of $\mathtt{NRMSE}$ among all marker axes.

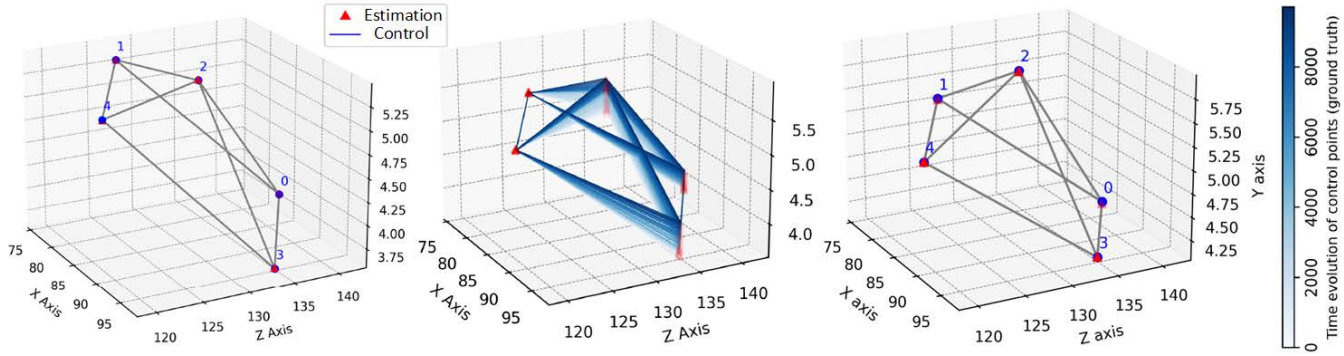

Fig. 5: Spatial representation of the pouch's state evolution over time for estimated points (red triangle) and control points (blue circle) for all markers. **Left**: the initial state, **Middle**: the estimated states, **Right**: the final state. Note that the edges are gradually colored from gray to blue, following the time steps evolution, where darker blue shows the closer to the final state. We denote the middle marker as *Marker 2*, and the markers at the four corners as *Marker 1*, *Marker 0*, *Marker 3*, and *Marker 4* clockwise. The axes are plotted in mm.

C. Real-Robot Experiments

1) Hardware & Software Setup: The Peltier elements of the liquid pouch actuator are connected to the $3.7\,\mathrm{V}$ output of a MOSFET-based switching circuit, which is controlled by an M5StickC PLUS2 [29]. The program in the microcontroller controls the Peltier elements to heat and cool the liquid pouch actuator, following random thermal cycling (as shown in Fig. 6A). One thermal cycle includes a pair of random heating time t_{on} and a random cooling time t_{off}:

- Heating time: $t_{\mathrm{on}} = \{1\,\mathrm{s}, 2\,\mathrm{s}, 3\,\mathrm{s}, \cdots, 40\,\mathrm{s}\}$
- Cooling time: $t_{\mathrm{off}} = \{5\,\mathrm{s}, 6\,\mathrm{s}, 7\,\mathrm{s}, \cdots, 15\,\mathrm{s}\}$

For each pair of $\{t_{\mathrm{on}}, t_{\mathrm{off}}\}$, we repeat the thermal cycle for $m = 5$ times. After that, the liquid pouch actuator is turned off for $m \times t_{\mathrm{pause}} = 5 \times 1.5\,\mathrm{s} = 7.5\,\mathrm{s}$ before starting the next pair of $\{t_{\mathrm{on}}, t_{\mathrm{off}}\}$. Fig. 6B shows snapshots of the inflation of a liquid phase change pouch actuator.

2) Real-World Performance of Method: To evaluate the method's real-world performance, we prepare the collected data from the OptiTrack setup to be ready for the *PhysRes* model with the number of the experiment (416 in total), the time-dependent values ($19,588$ points), and the coordinates (15 positional profiles for five markers with x, y, z). Analogously, the recorded markers' coordinates that serve as inputs into *PhysRes* are captured using the OptiTrack system with the same setup as in the data collection phase.

Specifically, each session corresponds to a different signal length (or heating time) between $1\,\mathrm{s}$ and $40\,\mathrm{s}$, as explained previously. We thus visually inspect to ensure that the markers' positions are consistent across all experiments

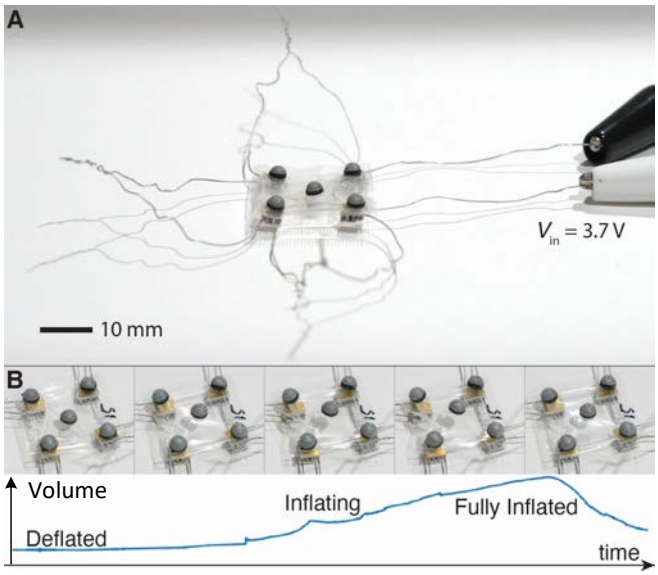

Fig. 6: (**A**) The liquid phase change actuator is driven by a power source $V_{\text{in}} = 3.7\,\text{V}$. An M5StickC PLUS2 microcontroller controls the timing of the thermal cycling through a MOSFET-based switch circuit. (**B**) The volumetric inflation profile of a liquid phase change pouch actuator, both in image frames and recorded data.

(markers 1, 0, 3, 4 are organized clockwise, and marker 2 is at the center), and discard any erroneous labeling, resulting in a final number of 399 experiments. The time-dependent coordinates are interpolated to have a fixed length for all experiments, matching the requirements of the model matrices. The collected data are then divided into a training set (70%) and a test set (30%), and randomized across 279 experiments for the training set and 120 experiments for the test set, so that the model does not learn patterns specific to the data collection's sequential nature. The input to the network consists of shifted coordinates by half of the points in the original array, while the other half indexes the target for model estimations (i.e., the input shifted ahead in time by 9,794 steps, half the total number of time steps). Then, the model is trained to reconstruct the pouch's state on the test set 9, 794 steps ahead. Fig. 4 shows how the estimations (in red) match the target (blue) from the test set input (green). The spatial representation of the pouch's time evolution is also shown in Fig. 5. From the results of both Fig. 4 and Fig. 5, we conclude that the network can model the states.

Nevertheless, due to the high nonlinearity of the actuator's liquid phase, the inflation states vary widely, even with an identical heating time. We highlight that such nonlinearity and the difficulty of controlling the pouch despite receiving the same signals are the primary motivations for this work.

We obtain a mean NRMSE of 0.00413 with a median NRMSE of 0.000159 for the network over 120 testing experiments. Fig. 7 shows that the trained model could accurately reconstruct the test set. We also obtain a median of 0.016% absolute percentage error for the volumetric state estimation, indicating accurate estimations of the volumetric state from the initial set of coordinates provided to *PhysRes*. The model provides us with more insights into the type of signal length to use for a real-world application of object

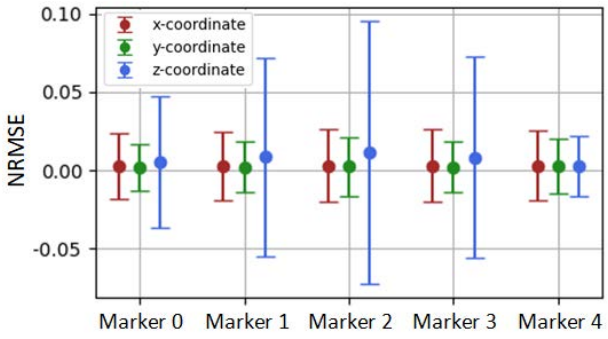

Fig. 7: Network error quantification with mean (μ) and standard deviation (σ) between estimated states and ground truth of all five markers across 120 testing experiments using *PhysRes*.

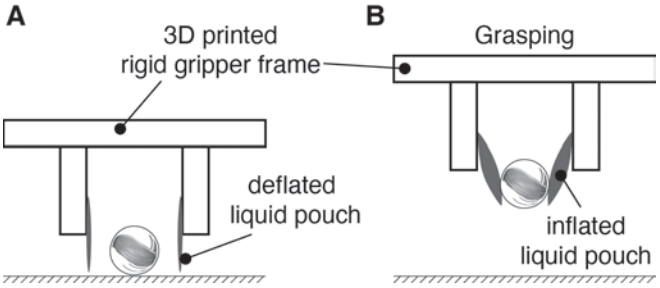

Fig. 8: Gripper with two liquid phase change pouch actuators as two fingers to grasp soft and delicate objects. (**A**) When the liquid pouch is deflated, the gripper is resting. (**B**) The gripper applies gripping force by inflating the pouch actuators to grasp the object.

picking, as discussed in the next section. For instance, longer heating signals do not lead to better inflations, while signals in the 20 s range are more reliable for the steady inflation required for grabbing, holding, and picking.

D. Demonstration: Gripper with Liquid Pouch Actuators

We demonstrate the application of our liquid-phase change pouch actuator modeling in a gripper made from two liquid pouch actuators, which can grasp soft and delicate objects, such as a tissue ball and a potato chip.

We attach two $20\,\text{mm} \times 20\,\text{mm}$ liquid phase change pouch actuators, serving as the fingers of the gripper, to a 3D-printed rigid gripper frame. When the liquid phase change pouch actuators are not activated, they are deflated and ready to approach the targeted object (Fig. 8A). Once the gripper is in the position that is ready to grasp, the two liquid phase change pouch actuators are activated and inflated to hold around the object, as shown in Fig. 8B. This gripper is attached to a robotic arm, as shown in Fig. 9A. The robotic arm lifts both the gripper and the object being grasped. The gripper is flexible enough to hold and pick up a deformable object like a tissue ball (Fig. 9B) and a brittle object like a potato chip (Fig. 9C).

V. DISCUSSION AND FUTURE WORKS

In this study, we deploy *PhysRes* as a physical reservoir computing-based method to estimate the volumetric states of a liquid phase change pouch actuator. This study demonstrates that the model can accurately represent the system states. Our findings hint at using the model to

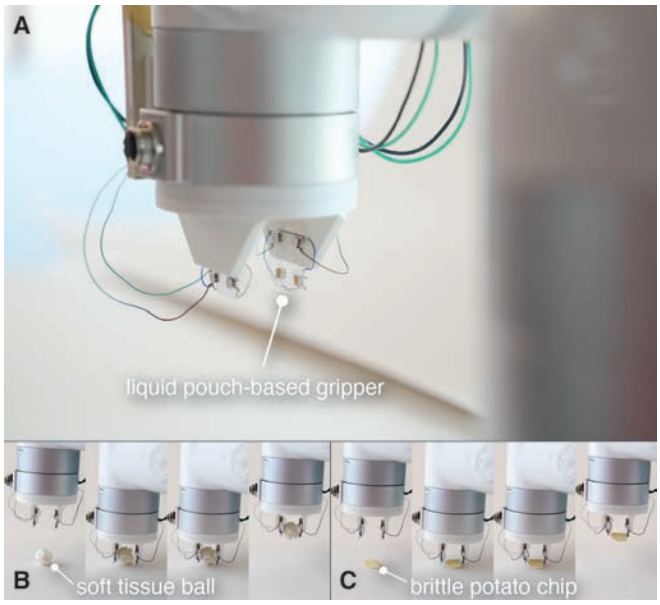

Fig. 9: (**A**) The two liquid phase change pouch actuators are attached to a 3D-printed robotic arm end-effector mount. (**B**) Grasping, holding, and picking up a soft tissue ball. (**C**) Grasping and picking up a brittle potato chip delicately.

estimate and provide control signals to the liquid phase change pouch actuators. The challenge of modeling and controlling soft actuators, particularly those with complex behaviors like phase change, is well-documented. Traditional approaches often rely on computationally intensive Finite Element Method (FEM) simulations or simplified analytical models that struggle to capture the full spectrum of nonlinear dynamics. We observed that the signal predicted by *PhysRes* appears relatively noisy compared to the local mean kernel. This apparent noise is primarily attributed to the small scale of variation in the data (particularly in the Z-direction, where fluctuations occur within a few tenths of a millimeter, at the limit of the accuracy threshold of the OptiTrack system), which then propagates into the model's state reconstruction. Rather than being mere noise, these details reflect the high sensitivity of our model, which successfully propagates these micro-dynamics into the state reconstruction. While we apply a Gaussian kernel to smooth the output for visualization purposes, the raw prediction's high fidelity to the ground truth makes *PhysRes* a promising candidate for applications requiring precise positional control. The development of a gripper demonstrates the practical utility of our state estimation model. While a comprehensive force control loop is a goal for future work, many robotic manipulation tasks, such as handling delicate or lightweight objects, prioritize precise positioning and gentle interaction over high force application. In the future, we will expand the work to build a closed-loop, stable control paradigm for liquid phase change pouch actuators based on different variations of reservoir computing.

Learning Control Parameters from An Expected Actuation: We will conduct more extensive experiments to build a reservoir computing-based network to learn the optimal controlling parameters for the liquid pouch's desired volumetric inflation/deflation.

Benchmarking with Different Reservoir Computing Variations: We will benchmark the performance of different variations of reservoir computing, such as ESN, LSM, and Hysteretic Reservoir.

Force Characterization and Multi-Modal Sensing: Our priority is to establish the relationship between the actuator's volumetric state and its force generation capability, a critical step for stable grasping and force-feedback control. We will collect additional non-linear output from the liquid phase change pouch actuators, such as temperature profile, to use as a physical reservoir for training the model. We will instrument the actuator to measure output forces, creating a comprehensive model that links volume to force, similar to characterization efforts for other soft actuators and building on recent advances in sensorless estimation techniques [30], [31]. Additionally, the relationship between the resulting volumetric state and the applied forces is being established to support future investigations in the areas of force control and grasping stability assessment.

Exploration of Model Transferability to Different Liquid Pouch Configurations: We will evaluate the performance of our learned model on liquid phase change pouch actuators with various sizes, shapes, and working environments (*e.g.*, pressurized, air, or underwater settings).

VI. CONCLUSIONS

In this paper, we explore the modeling of liquid phase change pouch actuators using *PhysRes*, our reservoir computing framework. We detail the design, hardware, and software pipeline for collecting data on the behavior of a Peltier elements-driven liquid phase change pouch actuator through multiple inflation/deflation cycles. We succeed in modeling the states of the system based on the observed inflation. This finding is one step closer to controlling non-linear systems that are well-suited for robotic applications, such as the liquid phase change pouch actuators we propose for our soft robotic gripper.

REFERENCES

[1] C. Caremel, Y. Kawahara, and K. Nakajima, "Hysteretic reservoir," *Phys. Rev. Appl.*, vol. 22, p. 064045, Dec 2024.

[2] B. Gorissen, D. Reynaerts, S. Konishi, K. Yoshida, J.-W. Kim, and M. De Volder, "Elastic inflatable actuators for soft robotic applications," *Adv. Mater.*, vol. 29, no. 43, p. 1604977, Nov. 2017.

[3] P. Polygerinos, N. Correll, S. A. Morin, B. Mosadegh, C. D. Onal, K. Petersen, M. Cianchetti, M. T. Tolley, and R. F. Shepherd, "Soft robotics: Review of fluid-driven intrinsically soft devices; manufacturing, sensing, control, and applications in human-robot interaction: Review of fluid-driven intrinsically soft robots," *Adv. Eng. Mater.*, vol. 19, no. 12, p. 1700016, Dec. 2017.

[4] L. Hines, K. Petersen, G. Z. Lum, and M. Sitti, "Soft actuators for small-scale robotics," *Adv. Mater.*, vol. 29, no. 13, p. 1603483, Apr. 2017.

[5] D. Drotman, M. Ishida, S. Jadhav, and M. T. Tolley, "Application-driven design of soft, 3D printed, pneumatic actuators with bellows," *IEEE ASME Trans. Mechatron.*, vol. 24, no. 1, pp. 1–1, 2018.

[6] R. F. Shepherd, F. Ilievski, W. Choi, S. A. Morin, A. A. Stokes, A. D. Mazzeo, X. Chen, M. Wang, and G. M. Whitesides, "Multigait soft robot," *Proc. Natl. Acad. Sci. U. S. A.*, vol. 108, no. 51, pp. 20 400–20 403, Dec. 2011.

[7] E. W. Hawkes, L. H. Blumenschein, J. D. Greer, and A. M. Okamura, "A soft robot that navigates its environment through growth," *Science Robotics*, vol. 2, no. 8, p. eaan3028, Jul. 2017.

[8] R. Niiyama, D. Rus, and S. Kim, "Pouch motors: Printable/inflatable soft actuators for robotics," in *2014 IEEE International Conference on Robotics and Automation (ICRA)*. IEEE, 2014, pp. 6332–6337.

[9] A. Miriyev, K. Stack, and H. Lipson, "Soft material for soft actuators," *Nat. Commun.*, vol. 8, no. 1, p. 596, Sep. 2017.

[10] K. Narumi, H. Sato, K. Nakahara, Y. ah Seong, K. Morinaga, Y. Kakehi, R. Niiyama, and Y. Kawahara, "Liquid pouch motors: printable planar actuators driven by liquid-to-gas phase change for shape-changing interfaces," *IEEE Robotics and Automation Letters*, vol. 5, no. 3, pp. 3915–3922, 2020.

[11] S. Hirai, T. Nagatomo, T. Hiraki, H. Ishizua, Y. Kawahara, and N. Miki, "Micro elastic pouch motors: Elastically deformable and miniaturized soft actuators using liquid-to-gas phase change," *IEEE Robotics and Automation Letters*, pp. 1–1, 2021.

[12] T. Hiraki, K. Nakahara, K. Narumi, R. Niiyama, N. Kida, N. Takamura, H. Okamoto, and Y. Kawahara, "Laser pouch motors: Selective and wireless activation of soft actuators by laser-powered liquid-to-gas phase change," *IEEE Robotics and Automation Letters*, vol. 5, no. 3, pp. 4180–4187, 2020.

[13] T. Exley, R. Wijesundara, N. Tan, A. Sunkara, X. He, S. Wang, B. Chan, A. Jain, L. Espinosa, and A. Jafari, "Agonist-antagonist pouch motors: Bidirectional soft actuators enhanced by thermally responsive peltier elements," *arXiv preprint arXiv:2403.10955*, 2024.

[14] R. Uramune, H. Ishizuka, T. Hiraki, Y. Kawahara, S. Ikeda, and O. Oshiro, "Hapouch: A miniaturized, soft, and wearable haptic display device using a liquid-to-gas phase change actuator," *IEEE Access*, vol. 10, pp. 16 830–16 842, 2022.

[15] T. D. Ta, Z. Chang, K. Narumi, T. Umedachi, and Y. Kawahara, "Printable origami bistable structures for foldable jumpers," in *2022 International Conference on Robotics and Automation (ICRA)*. IEEE, May 2022.

[16] C. Caremel, M. Ishige, T. D. Ta, and Y. Kawahara, "Echo state network for soft actuator control," *Journal of Robotics and Mechatronics*, vol. 34, no. 2, pp. 413–421, 2022.

[17] J. Shen, T. Miyazaki, and K. Kawashima, "Control pneumatic soft bending actuator with feedforward hysteresis compensation by pneumatic physical reservoir computing," *IEEE Robotics and Automation Letters*, 2024.

[18] M. Nakajima, Y. Zhang, K. Inoue, Y. Kuniyoshi, T. Hashimoto, and K. Nakajima, "Reservoir direct feedback alignment: deep learning by physical dynamics," *Communications Physics*, vol. 7, no. 1, p. 411, 2024.

[19] H. Jaeger, "The "echo state" approach to analysing and training recurrent neural networks-with an erratum note," *Bonn, Germany: German National Research Center for Information Technology GMD Technical Report*, vol. 148, no. 34, p. 13, 2001.

[20] W. Maass, T. Natschläger, and H. Markram, "Real-time computing without stable states: A new framework for neural computation based on perturbations," *Neural Computation*, vol. 14, no. 11, pp. 2531–2560, 2002.

[21] R. de Azambuja, F. B. Klein, S. V. Adams, M. F. Stoelen, and A. Cangelosi, "Short-term plasticity in a liquid state machine biomimetic robot arm controller," in *2017 International Joint Conference on Neural Networks (IJCNN)*. IEEE, 2017, pp. 3399–3408.

[22] T. Li, K. Nakajima, M. Cianchetti, C. Laschi, and R. Pfeifer, "Behavior switching using reservoir computing for a soft robotic arm," in *2012 IEEE International Conference on Robotics and Automation*. IEEE, 2012, pp. 4918–4924.

[23] K. Nakajima, H. Hauser, R. Kang, E. Guglielmino, D. G. Caldwell, and R. Pfeifer, "A soft body as a reservoir: case studies in a dynamic model of octopus-inspired soft robotic arm," *Frontiers in computational neuroscience*, vol. 7, p. 91, 2013.

[24] K. Nakajima, "Physical reservoir computing—an introductory perspective," *Japanese Journal of Applied Physics*, vol. 59, no. 6, p. 060501, 2020.

[25] R. Sakurai, M. Nishida, H. Sakurai, Y. Wakao, N. Akashi, Y. Kuniyoshi, Y. Minami, and K. Nakajima, "Emulating a sensor using soft material dynamics: A reservoir computing approach to pneumatic artificial muscle," in *2020 3rd IEEE International Conference on Soft Robotics (RoboSoft)*. IEEE, 2020, pp. 710–717.

[26] J. Wang, Z. Qiao, W. Zhang, and S. Li, "Proprioceptive and exteroceptive information perception in a fabric soft robotic arm via physical reservoir computing with minimal training data," *Advanced Intelligent Systems*, p. 2400534, 2024.

[27] Zhejiang Noah Fluorochemical Co., Ltd., "Noah® 7100 Electronic cleaning agent," https://www.zjnoah.cn/index.php?m=content&c=index&a=show&catid=79&id=11#texing, 2021, [Online; accessed 19-February-2025].

[28] Marlow Industries, Inc., "Peltier Element NL1010T-01AC," https://www.digikey.com/en/products/detail/coherent-thermal-solutions/NL1010T-01AC/6159071, 2025, [Online; accessed 19-February-2025].

[29] M5Stack Technology Co., Ltd., "M5StickC Plus 2," 2021, [Online; accessed 23-February-2025].

[30] T. Kanno and K. Kawashima, "External force estimation of pneumatic soft actuator with built-in displacement sensor," *Sensors and Materials*, vol. 33, p. 555, 02 2021.

[31] S. Joshi and J. Paik, "Sensorless force and displacement estimation in soft actuators," *Soft Matter*, vol. 19, pp. 2554–2563, 2023.